Ultrahigh-intensity optical slow-wave structure for direct laser electron acceleration

Andrew G. York,* B. D. Layer, J. P. Palastro, T. M. Antonsen, and H. M. Milchberg

Institute for Research in Electronics and Applied Physics, University of Maryland, College Park, College Park, Maryland 20742, USA
**Corresponding author: Andrew.G.York+JOSAB@gmail.com*

Received January 3, 2008; revised April 14, 2008; accepted April 18, 2008; posted April 23, 2008 (Doc. ID 91142); published June 4, 2008

We report the development of corrugated slow-wave plasma guiding structures with application to quasi-phase-matched direct laser acceleration of charged particles. These structures support guided propagation at intensities up to 2×10^{17} W/cm^2, limited at present by our current laser energy and side leakage. Hydrogen, nitrogen, and argon plasma waveguides up to 1.5 cm in length with a corrugation period as short as 35 μm are generated in extended cryogenic cluster jet flows, with corrugation depth approaching 100%. These structures remove the limitations of diffraction, phase matching, and material damage thresholds and promise to allow high-field acceleration of electrons over many centimeters using relatively small femtosecond lasers. We present simulations that show that a laser pulse power of 1.9 TW should allow an acceleration gradient larger than 80 MV/cm. A modest power of only 30 GW would still allow acceleration gradients in excess of 10 MV/cm.

OCIS codes: 350.5400, 350.3950, 230.7380, 320.7160.

1. INTRODUCTION

Laser wakefield acceleration [1–3] of electrons to relativistic velocities is often described as a tabletop experiment [4], promising to make high-energy electrons available outside of large, multiuser accelerator facilities. Recent advances in wakefield acceleration have produced monoenergetic beams [5–7] and impressive electron energies exceeding 1 GeV [8]. These experiments, however, all use expensive multiterawatt laser systems that cannot reasonably be considered tabletop. Direct laser acceleration is an attractive alternative for producing relativistic electrons. Wakefield acceleration is a nonlinear process and is inefficient at subterawatt powers, but direct laser acceleration (a linear process) has no threshold intensity. Small, inexpensive few-millijoule chirped-pulse regenerative amplifiers that could never reach the intensity threshold for wakefield acceleration could still be used for direct laser acceleration.

We describe experimental [9] and theoretical [10] progress toward a practical scheme for direct electron acceleration at multi-MeV/cm gradients by subterawatt femtosecond pulsed lasers. Just as the segmented copper structure of the Stanford Linear Accelerator channels the megawatt power of microwave-frequency klystrons to accelerate electrons over several kilometers [11], we have created a corrugated plasma structure to guide the gigawatt or terawatt power of optical frequency femtosecond pulses over centimeters. Our simulations show that if this structure is correctly tuned and injected with a radially polarized laser beam and a simultaneously copropagating electron bunch, true tabletop electron acceleration is possible: A laser pulse power of 1.9 TW should allow an acceleration gradient larger than 80 MV/cm, and a modest power of only 30 GW would still allow acceleration gradients in excess of 10 MV/cm.

2. CORRUGATED PLASMA WAVEGUIDE

Ultraintense laser–plasma interaction applications including x-ray lasers, coherent electromagnetic wave generation [12–15], and electron acceleration by laser-driven wakefields [1–3] all rely on the extended diffraction-suppressed propagation of extreme-intensity laser pulses in plasma optical guiding structures to achieve high efficiency. Plasma is unavoidable at laser intensities well in excess of the ionization threshold of any atom or molecule. The optical mode structure and dispersion properties of plasma waveguides have been discussed in detail [16].

Beyond confinement of beam intensity, waveguide control of beams can be augmented by additional branches to the ω versus k dispersion diagram, where $k=k(\omega)$ is the axial wavenumber of the guide and ω is the angular frequency. Adding an axial (z) modulation of period d through variations in geometry, materials, or both gives rise to a wider class of solutions $u(\mathbf{r}_\perp,z,\omega)\exp(\imath kz)$, where $u(\mathbf{r}_\perp,z+d,\omega)=u(\mathbf{r}_\perp,z,\omega)$ and $k=k_c(\omega)+2\pi m/d$ (from the Floquet–Bloch theorem), where u is an electromagnetic field component, $\mathbf{r}_\perp$ is the transverse position, m is an integer, and k_c is the fundamental axial wavenumber [17]. The extra dispersion branches arise from the multiplicity of k values assigned to each ω for each transverse mode.

Two examples of modulated guiding structures illustrate low-intensity applications. In radio frequency accelerators (for example, SLAC [11]), charged particles are accelerated by the E_z field of a TM wave guided in an axially modulated copper waveguide. In an ordinary unmodu-

lated metal waveguide, guided-wave phase velocity $v_p = \omega/k$ is greater than c, so a charged particle would be accelerated and then decelerated as the wave oscillations pass the particle, giving zero net acceleration. However, a modulated structure can have an effective k, as discussed above, large enough to give $v_p < c$ so that the particle and wave speeds can be matched. Called a slow-wave structure, this type of guide finds wide application in both accelerators and microwave sources [17].

Another view of this matched interaction—called quasi phase matching—is that the wave speeds up and slows down in successive half-periods of the modulation in such a way that the partial acceleration in the first half is not completely canceled by deceleration in the second half. For a number of applications, quasi phase matching is enabled not only by the modulations in linear dispersion but also by the accompanying laser intensity modulations. In low-intensity guided-wave optics, periodic modulation in the material's optical nonlinearity or refractive index makes possible the quasi-phase-matched generation of low-order harmonics of the fundamental pump wave [18–21]. At higher intensity ($\sim 10^{14}$–10^{15} W/cm^2), modulated, gas-filled hollow core fibers have been used for the generation of extreme-ultraviolet high harmonics [22].

We recently achieved the first ever high-intensity optical guiding in an extended corrugated plasma slow-wave structure. The application of these structures to coherent electromagnetic-wave generation was first discussed in [23]. Spontaneous but uncontrolled modulated channels were reported in [24]. We have produced exceptionally stable plasma waveguides with adjustable axial modulation periods as short as 35 μm, where the period can be significantly smaller than the waveguide diameter. The axial modulations can also be extremely sharp and deep, with nearly 100% modulation in plasma density. We have measured guided propagation at intensities up to 2×10^{17} W/cm^2, limited only by our current laser energy and waveguide leakage.

Figure 1 shows the experimental setup. Initially, unmodulated waveguides were generated in cluster jets [25] using lowest-order (J_0) Bessel beam pulses produced by an axicon-focused beam from a 10 Hz, 1064 nm, 100 ps Nd:YAG laser with a pulse energy of 200–500 mJ.

The cluster source in these experiments was a cryogenically cooled supersonic gas jet with a 1.5 cm long by 1 mm wide nozzle exit orifice [9]. The 25 mm line-focus length of the Bessel beam overlapped the 1.5 cm length of the cluster jet, resulting in 1.5 cm long plasma channels. Waveguides were injected at $f/10$ through a hole in the axicon [Fig. 1(a)] with a 70 mJ, 70 fs, 800 nm Ti:sapphire laser pulse synchronized [26] and delayed with respect to the channel-generating Nd:YAG pulse. A small portion of this pulse ($\sim$1 mJ) was split off into a delay line, directed transversely through the waveguide, and then imaged through a femtosecond folded-wavefront Michelson interferometer onto a CCD camera. Electron density profile images of the evolving corrugated waveguide were obtained by phase extraction of the time-resolved interferograms, followed by Abel inversion.

To impose axial modulations on the plasma channel, a transmissive ring grating (RG) and associated imaging optics were centered in the path of the Nd:YAG laser pulse. The RGs used in these experiments were lithographically etched fused-silica disks with variable groove period, groove structure, and duty cycle. The ring grating shown in Fig. 2(b), used to generate the waveguide shown in Fig. 1(c), is a set of concentric rings regularly spaced with a radial period of 10 μm, a groove depth of 1 μm, and a duty cycle of $\sim$70%. The axicon projects the diffraction pattern produced by the RG onto the optical axis, leading

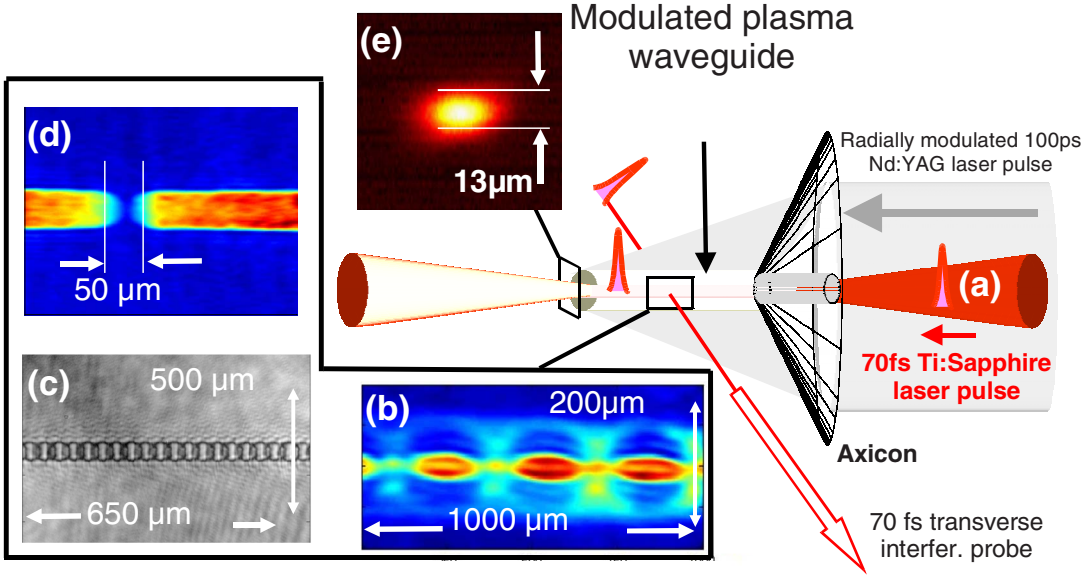

Fig. 1. (Color online) Experimental geometry: Radially modulated Nd:YAG laser pulse (200–500 mJ, 100 ps, 1064 nm) from a ring grating imaging system (not shown) focused by an axicon onto a liquid-nitrogen-cooled elongated cluster jet target, generating a 1.5 cm long corrugated plasma channel. (a) Ti:sapphire laser pulse guided down the channel at an adjustable delay with respect to the Nd:YAG pulse. A 1 mJ portion of the 70 fs, 800 nm pulse was directed transversely through the corrugated guide and into a folded wavefront Michelson interferometer for time-resolved interferometric and shadowgraphic images. Phase images of channels with (b) a 300 μm modulation period in argon clusters; (c) a 35 μm period in air; and (d) a single, deep corrugation in nitrogen clusters. (e) Lowest-order exit mode from the guide of Fig. 3(b)(1ii).

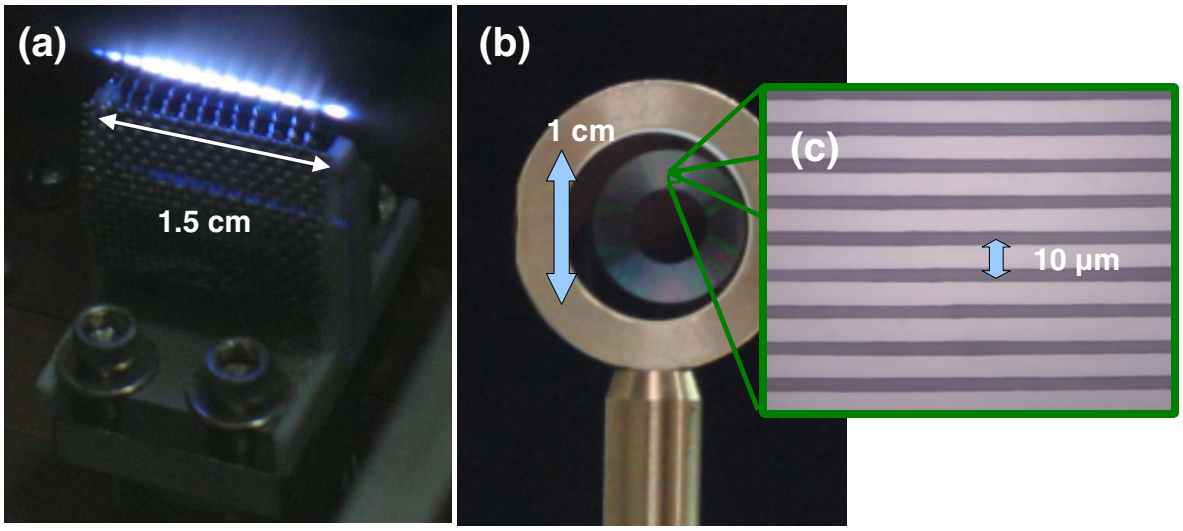

Fig. 2. (Color online) Different corrugation methods: (a) Wire mesh obstructing cluster jet flow, producing a waveguide with an ~1 mm corrugation period and near 100% density modulation. (b) Transmissive ring grating used to produce the waveguide shown in Fig. 1(c). This corrugation method modulates ionization and heating rather than material density. High-magnification image of the ring grating (c) shows the ~10 μm groove period required to produce periodic ~35 μm corrugations.

to axial intensity modulations of the Bessel beam. The dominant axial modulation of the central spot intensity imposes axial modulations in the heating and plasma generation in the cluster jet. For the present work, we imposed a periodic modulation, but arbitrary RG patterns are possible. Phase-matching direct laser acceleration of ions or nonrelativistic electrons, for example, would require a graded modulation period.

Alternatively, the plasma channel can be corrugated by obstructing the flow of clusters from the gas jet. Figure 1(d) shows the effect of placing a single 25 μm diameter tungsten wire directly between the jet nozzle and the focus of the Bessel beam. The resulting corrugation is extremely sharp owing to the big reduction of clusters in the shadow region. Guiding an intense femtosecond pulse in this channel reveals no measurable scattering or ionization in this gap.

These two methods of corrugation offer complementary strengths. RG-generated corrugations are computer designed, easy to align, and extremely precise and regular, but cannot be tuned much without switching ring gratings. Wire-generated corrugations, on the other hand, can be easily adjustable in the laboratory. RG-generated corrugations modulate heating, so they tend to produce channels with strong modulation in diameter [Fig. 1(b)], whereas wire-generated corrugations strongly modulate density without affecting waveguide diameter much at all [Fig. 1(d)]. Our simulations of laser acceleration in these channels have focused on density modulations for mathematical simplicity, but diameter modulation could have important effects on acceleration gradients.

The 100 ps heater pulse is essentially an impulse on the hydrodynamic time scale (~0.1–0.5 ns) of the heated bulk plasma (formed from merged cluster explosions) that

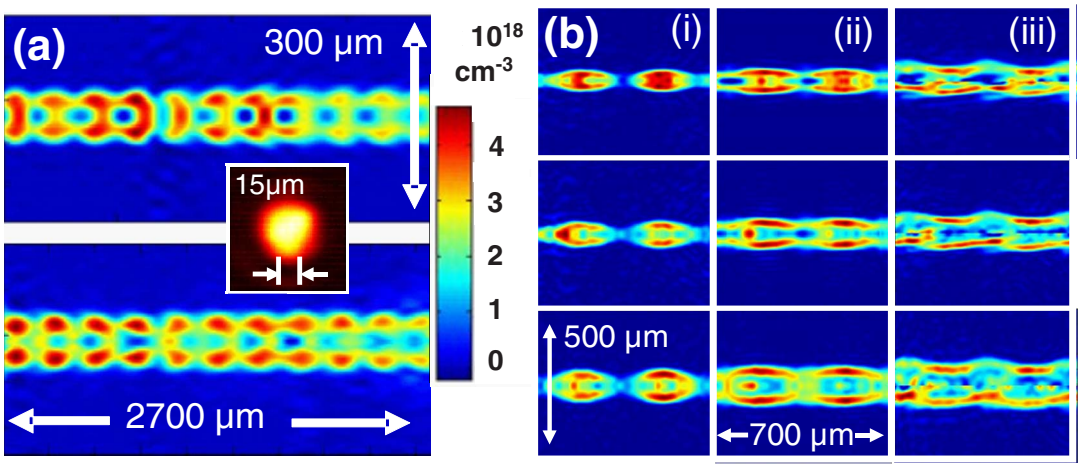

Fig. 3. (Color online) Corrugated channels produced in a hydrogen cluster jet at 800 psi and −145°C backing pressure and temperature. (a) ~3 mm section of the channel without (top panel) and with (bottom panel) injection at 1 ns delay of a 70 mJ, 70 fs, 800 nm laser pulse, viewed 100 ps after pulse passage. The channel exit mode of $w_{\mathrm{hwhm}}=15$ μm is shown in the inset. (b) Higher-magnification Abel-inverted electron density profiles of two corrugation periods for channel creation pulse energies of (i) 200, (ii) 300, and (iii) 500 mJ (with RG–axicon misalignment) at interferometer probe delays of, top to bottom, 0.5, 1, and 2 ns.

remains after the pulse [25]. This plasma then undergoes axially periodic radial hydrodynamic shock expansion, producing a corrugated plasma waveguide. Two examples of phase images of the magnified central waveguide region are shown in Fig. 1, with 300 μm RG-generated modulations in argon clusters [Fig. 1(b)] and a 25 μm wire-generated corrugation in nitrogen clusters [Fig. 1(d)]. Corrugated guides can also be generated in backfill gases: Fig. 1(c) shows a shadowgram of a modulated channel produced in air with a period of 35 μm. A typical guided exit mode from a modulated cluster plasma channel is shown in Fig. 1(e). Note that the cluster-generated channels are highly stable and reproducible: The shot-to-shot extracted density variation is less than 5%.

Figure 3 shows results for a corrugated hydrogen plasma waveguide. Hydrogen plasma waveguides are attractive for laser-plasma acceleration [1–3] because they are easily fully ionized during their formation, making impossible further ionization by guided intense pulses, which can lead to distortion and ionization-induced refractive defocusing. The modulation period $d \approx 300\ \mu$m was chosen to ensure clearly observable periodic oscillations in laser intensity. Figure 3(a) shows the electron density $N_e(r,z)$ of a 3 mm section near the entrance of a 1.5 cm hydrogen waveguide, 1 ns after generation. The density profiles are very similar in the injected (bottom) and uninjected (top) waveguides, showing that little change to the guide was produced by the guided pulse. With modulated hydrogen guides, energy throughput is ~10%, yielding an output intensity of 10^{17} W/cm^2. The low throughput is due to leakage and side scattering out of the guide due to the modulations. This leakage is directly seen in argon results. Figure 3(b) shows higher magnification profiles of two modulation periods as a function of interferometer probe pulse delay (0.5, 1, and 2 ns) for channel creation pulse energies of (i) 200 and (ii) 300 mJ. It is seen that lower pulse energy [(i)] can produce periodic beads of plasma, separated by zones of neutral clusters/atoms, whereas higher energy [(ii)] results in a more continuous channel. The beads act as plasma lenslets, collecting the light emerging from a neutral gap and focusing the beam into the next gap. Figure 3(b) (iii) shows the result of an intentional misalignment (at 500 mJ) of the Bessel beam axis and the RG optical axis: A continuous plasma fiber is generated with angular fluting.

Channels with higher ionization Z were generated in argon cluster jets. Figure 4(a) shows an extended region of channel at 1.5 ns delay with and without guided pulse injection (bottom and top panels, respectively) for a probe delay of ~10 ps after guided pulse passage. It is seen that the channel itself is little affected by the guided pulse, but in contrast to the hydrogen results, there is a significant electron density halo located at a radial distance ~100 μm from the channel. Short interval sequences of probe images show that the halo propagates right to left at the speed of light with the guided pulse. The halo radial position remains constant over the full 1.5 cm length of the corrugated channel but decays in density, suggesting that it originates from additional cluster ionization from channel side leakage [16] rather than from uncoupled entrance light skimming the outside of the channel. The leakage light moves radially across a zone of low-density plasma and neutrals until it reaches the layer of argon clusters that was unperturbed during channel formation. With hydrogen, the clusters are smaller and more fragile, so it is unlikely they survive so close to the channel after its formation, and hence there is no observed halo in Fig. 3.

Higher-resolution images of three periods of modulation near the argon channel center are shown in Fig. 4(b), for cases of beaded (300 mJ pump, left column) and continuous (500 mJ pump, right column) modulations, without guided pulse injection [panels (1)] and with injection

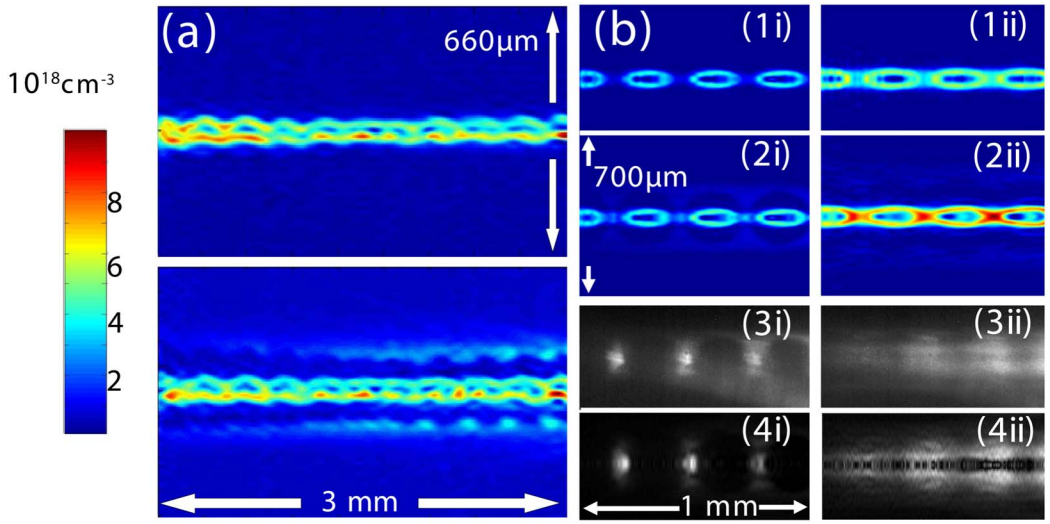

Fig. 4. (Color online) Corrugated channels in an argon cluster jet at 800 psi backing pressure and room temperature. Laser 70 mJ, 70 fs, 800 nm. (a) 3 mm section of channel without (top panel) and with (bottom panel) injection at 1.5 ns delay. (b) Magnified images at 2 ns delay of beaded (300 mJ pump, left column) and more continuous (500 mJ pump, right column) channel modulations. Left and right columns: (1) density profile of uninjected guide, (2) density profile of injected guide, (3) guided scattering image at 800 nm corresponding to (2), (4) Abel inversion of (3).

[panels (2)–(4)]. In the case of the beaded guide, Fig. 4(b)(2i) shows strong additional ionization by the guided pulse in the neutral gaps as the beam is focused by each plasma lenslet and collected by the next. Remarkably in this case, the overall channel coupled-energy throughput is still 10%, showing that there is significant injection and capture of light by successive lenslets over the full 1.5 cm length of the channel. Throughput for the continuous modulation case is 20%, yielding 2×10^{17} W/cm^2 peak intensity at a beam waist, using the fact that the beam exits the channel at a guide bulge. By comparison, throughput for this injection delay in unmodulated waveguides is 60%. Panels (2) both show in more detail the ionization halo induced by side leakage of the guided pulse. Side-imaged Thomson–Rayleigh scattering of guided 800 nm light shows scattering strongly localized from cluster ionization at the neutral gaps in the beaded guide [Fig. 4(b)(3i)] and more smoothly modulated from leakage at the beam waists in the more continuous guide [Fig. 4(b)(3ii)]. Panels (4i) and (4ii), which show the scattering source (r,z) profiles, are Abel inversions of panels (3i) and (3ii). These images make clear that the dominant scatterers are likely clusters, either those surviving in the gaps between beads or those external to the continuously modulated guide.

Detailed images of wire-generated corrugations are shown in Fig. 5. A 25 μm diameter tungsten wire placed just above the gas jet nozzle produces a sharp density notch in the cluster target. The phase images shown in Fig. 5 show that this 50 μm density notch is persistent in liquid-nitrogen-cooled nitrogen clusters [Fig. 5(b)] and room-temperature argon clusters [Fig. 5(c)] as the waveguide expands over more than 2 ns. Figure 5(a) is the Abel-inverted electron density of the 1 ns delay phase image from Fig. 5(b). The electron density peaks at approximately 9×10^{18} cm^{-3} at the channel wall and falls to below the noise floor of our measurement in the middle of the 50 μm corrugation. The 60 μm waveguide diameter, however, is nearly unchanged, in contrast to RG-generated corrugations. Guiding a 70 mJ, 70 fs, 800 nm laser pulse in these structures shows no further scattering from this gap, indicating the absence of clustered or unclustered gas rather than a simple ionization modulation.

Future experiments will explore extended wire-modulated guides and attempt to reduce leakage of the guided pulse. However, we note that even with the ~80% leakage shown here, the guided laser field at the channel exit is reduced by only ~50% from that at the entrance.

3. DIRECT LASER ACCELERATION OF ELECTRONS IN THE CORRUGATED-PLASMA WAVEGUIDE

A wide variety of structures have been used to allow the exchange of energy between radiation and relativistic electrons, from a multi-kilometer-long microwave-frequency copper waveguide [11] to a hydrogen-filled gas cell fed by a conically focused, radially polarized nanosecond CO_2 laser [27] to a simple reflective metal tape positioned at the focus of a picosecond laser [28]. Although the efficiency and expense of these schemes varies greatly, the electron acceleration gradients they can achieve are ultimately limited by the radiation intensity they can produce and control and typically are significantly less than 1 MV/cm. Modern femtosecond lasers based on chirped-pulse amplification [29] can produce focused field strengths in excess of 10 GV/cm. An accelerating structure that could control this field strength would allow enormous acceleration gradients, but no material can survive this intensity un-ionized. The corrugated-plasma waveguide, however, is already ionized and can control laser pulse propagation to allow efficient electron acceleration, as illustrated in Fig. 6. Our simulations show that in this structure a laser pulse power of 1.9 TW yields an acceleration gradient of 84 MV/cm, and only 30 GW still yields an acceleration gradient of 10.6 MV/cm.

Using uncorrugated plasma waveguides [16] for direct electromagnetic acceleration has been suggested by Serafim *et al.* [30], who proposed guiding a radially polarized laser pulse to accelerate a copropagating relativistic electron bunch. The laser's dominant radial component E_r guides as a hollow mode with peak intensity at $r=w_{ch}/\sqrt{2}$, where the mode radius w_{ch} is given by $w_{ch}=(1/\pi r_e\Delta N_e)^{1/2}$, r_e is the classical electron radius, and ΔN_e is the electron density difference between $r=0$ and $r=w_{ch}$. The accelerating field is the associated axial component E_z, which peaks at $r=0$ and passes through zero at $r=w_{ch}$. Following [30], the peak axial acceleration gradient from hollow beam guiding in a plasma channel is given by $E[\mathrm{GV/cm}]=98\lambda P^{1/2}/w_{ch}^2$, where W_{ch} and λ (laser wavelength) are in μm, and P is the peak laser power in TW. For a 1.9 TW laser pulse with $\lambda=800$ nm in a channel supporting $w_{ch}=15$ μm, E_z is an impressive 0.49 GV/cm.

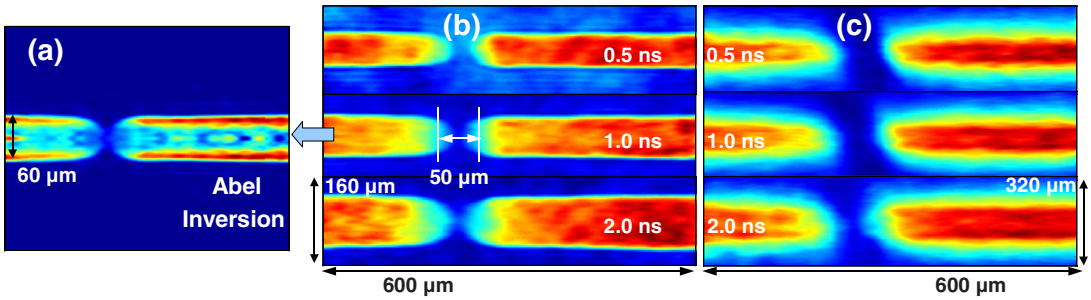

Fig. 5. (Color online) Abel-inverted electron density (a) of a wire-generated corrugation in nitrogen clusters 1 ns after creation shows nearly 100% density modulation. Phase images of these corrugations at 0.5, 1.0, and 2.0 ns delay in (b) nitrogen and (c) argon clusters show that this sharp density structure persists for the entire useful life of the waveguide.

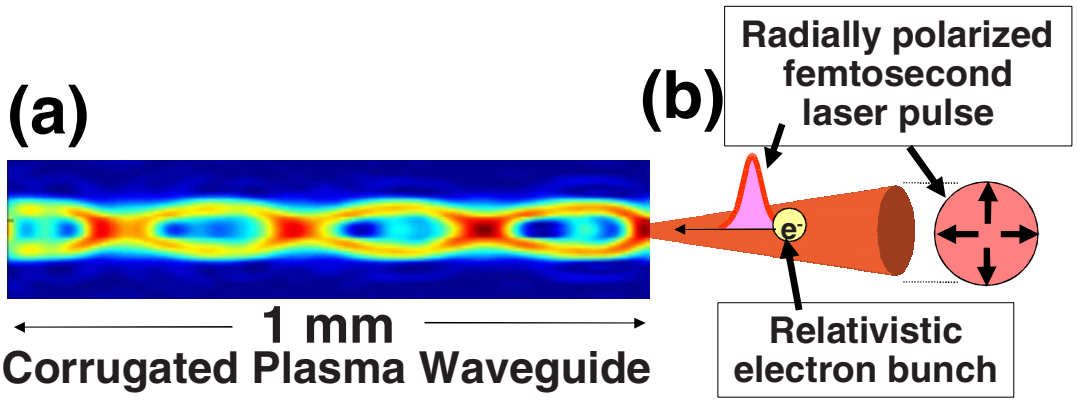

Fig. 6. (Color online) Direct acceleration of electrons by a femtosecond laser pulse in a corrugated plasma waveguide. (a) A hollow optical waveguide with corrugations in the guiding direction allows fine velocity control of guided radiation. (b) A radially polarized femtosecond laser pulse and a relativistic electron bunch are injected into this waveguide. If the corrugation period is matched to L_d, the laser pulse can accelerate these electrons.

If there were no slippage between the laser phase velocity and the electron velocity (essentially c), this would compare very favorably to laser wakefield acceleration: Malka *et al.* [3] used a 30 TW laser to produce an acceleration gradient of 0.66 GV/cm (200 MV over 3 mm). A regenerative amplifier with 1 mJ output can easily produce 20 GW of peak power, yielding a 49 MV/cm gradient. Of course, a means must be found to slow the laser phase velocity to c or less to match the relativistic electron velocity. Neutral gas as proposed in [30] will not survive the laser intensities essential for high values of accelerating field E_z; even pulses well below the terawatt level will propagate in fully ionized waveguides. Without neutral gas, the laser phase velocity in an uncorrugated plasma waveguide is strictly superluminal: A relativistic electron would slip 2π out of phase with the accelerating pulse after propagating a dephasing length $L_d = \lambda(N_0/N_{cr} + 2\lambda^2/\pi^2 w_{ch}^2)^{-1}$ [31], where N_0 is the on-axis plasma electron density of the channel and N_{cr} is the critical plasma electron density for wavelength λ. The electron receives no net acceleration: It would accelerate for a distance $L_d/2$, then decelerate an equal amount over the next $L_d/2$.

Figure 6(a) shows how the corrugated plasma waveguide can quasi phase match this interaction. Laser phase velocity is locally faster in high-plasma-density regions and slower in low plasma density. If L_d and the corrugation period are matched, the symmetry between acceleration and deceleration in a dephasing cycle is broken, and a properly phased electron will gain net energy; this process can be viewed as the inverse of transition radiation [32].

The use of a radially polarized laser pulse rather than simple linear polarization, as shown in Fig. 6(b), is crucial for accelerating high-quality electron beams. At the center of a cylindrically symmetric radially polarized beam, the accelerating force is maximized and transverse forces vanish. A cylindrically symmetric electron beam fits nicely in this high-gradient region, and electrons that make small excursions from the center of the beam can feel a time-averaged restoring force back to the beam center [10]. An electron beam injected into the center of a linearly polarized waveguide mode, however, would experience transverse forces that dwarf the longitudinal acceleration and be quickly expelled from the waveguide.

We obtain physical insight into the quasi-phase-matching process from finite-difference time-domain simulations of linear pulse propagation in the simplified plasma density shown in Fig. 7(a). This simulation was performed using a freely available software package with subpixel smoothing for increased accuracy [33]; assumes cylindrical symmetry; and includes plasma dispersion, finite pulse duration, and pulse leakage out of the channel. Finite computing resources force us to use an unrealistically long wavelength of 6.4 μm, so the waveguide density was scaled to make the laser phase velocity comparable to experimental conditions. Figure 7(b) shows the relative longitudinal and Fig. 7(c) the transverse electric field (scaled for visibility) felt by a relativistic ($v_z = c$) electron copropagating with the laser pulse nearly on axis. The transverse force depends strongly on the electron's transverse position; a truly on-axis electron would experience no transverse force due to the cylindrical symmetry of a radially polarized beam. The channel's corrugation period is matched to L_d, and the initial phase between the electron and the laser field is chosen so that the electron is accelerated in the low-density section of each corrugation. Phase velocity is lower in these regions, so dephasing is slower and the electron spends more than half of each L_d in phase with the accelerating field.

This simple picture is complicated somewhat by the modulation in waveguide diameter, which causes additional modulations in the guided pulse phase and intensity, but the electron clearly gains more energy during acceleration than it loses during deceleration. Each oscillation in Fig. 7(b) represents one dephasing cycle, and the number at each half-cycle is proportional to the energy gained or lost by the electron in that region. The transverse electric field shown in Fig. 7(c) is similarly quasi phase matched, which contributes to a net radial focusing–defocusing force. The laser group velocity is subluminal; the electron starts behind the laser pulse and overtakes it. This pulse-length dephasing limits the interaction length. Leakage of the laser pulse out of the waveguide is minimal, and plasma dispersion does not interfere with acceleration.

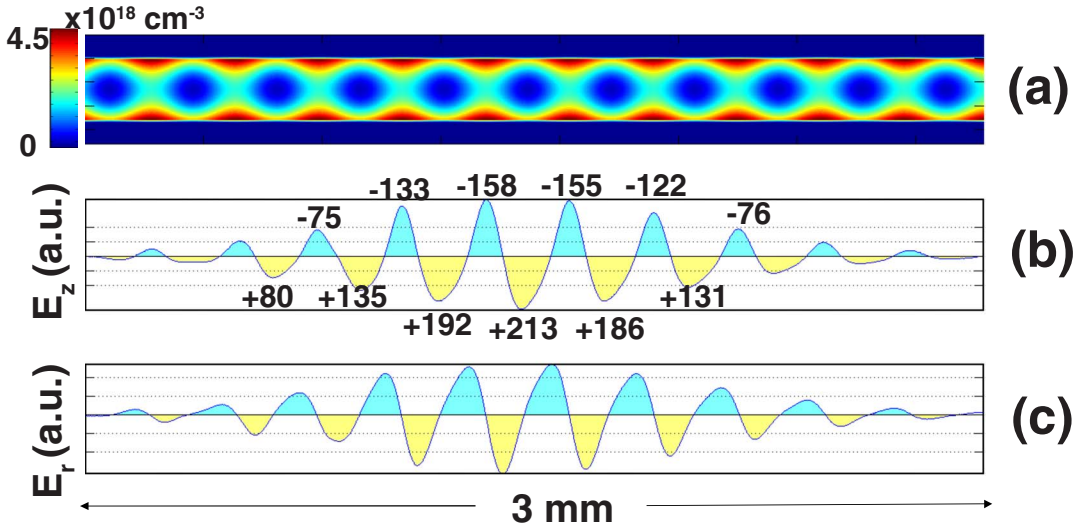

Fig. 7. (Color online) We approximate the plasma waveguide shown in Fig. 6(a) with (a) a simple electron density profile to model laser pulse propagation and electron acceleration. FDTD simulation results show (b) accelerating and (c) focusing forces felt by a properly phased relativistic ($v=c$) electron copropagating with a femtosecond laser pulse. Several acceleration (yellow) and deceleration (blue) half-dephasing cycles in (b) are labeled to show the work done on the electron in that region, with acceleration clearly dominating. The focusing force (c) is similarly quasi phase matched for this electron, to a lesser degree.

Starting from these encouraging results, we introduce an analytic model neglecting leakage and dispersion (which are less pronounced for a shorter wavelength) in order to study more realistic parameters. We start with the radial component of the laser vector potential:

$$A_r = \hat{A}_r(r,z,t)\exp[\iota(k_0 z - \omega_0 t)] + \text{c.c.}, \tag{1}$$

where k_0 and ω_0 are the central wavenumber and frequency of the laser pulse, respectively, and $\hat{A}_r(r,z,t)$ is a slowly varying envelope. We assume the pulse is azimuthally symmetric and consider plasma channels with low electron densities such that the plasma frequency satisfies $\omega_p \ll \omega_0$, where $\omega_p^2 = 4\pi e^2 N_e(r,z)/m_e$, $-e$ is the electron charge, m_e is the electron mass, and N_e is the electron density. In this regime the envelope $\hat{A}_r$ evolves on a time scale much longer than the laser period. The slowly varying envelope equation then determines the evolution of the laser pulse:

$$\left[2\,\iota k_0\left(\frac{\partial}{\partial z} + \frac{1}{c}\frac{\partial}{\partial t}\right) + \frac{1}{r}\frac{\partial}{\partial r}r\frac{\partial}{\partial r} - \frac{1}{r^2}\right]\hat{A}_r = \frac{\omega_p^2(r,z)}{c^2}\hat{A}_r, \tag{2}$$

where $\omega_0 = k_0 c$, and we have assumed that the electron plasma responds as a linear nonrelativistic cold fluid. Because the laser-electron dephasing length L_d depends on the electron's velocity [31], acceleration of subrelativistic electrons requires a structure with a graded modulation period to ensure L_d remains matched to the modulations over the entire interaction length. For mathematical simplicity we consider a fixed modulation period, suited to acceleration of electrons with $\gamma \gg 1$ for which the relativistic electron velocity depends only weakly on γ and L_d is nearly constant. We limit our analysis to a periodic electron density profile $N_e(r,z) = N_0[1 + \delta\sin(k_m z)] + N_0'' r^2/2$, where δ is the relative amplitude of the density modulation, N_0'' determines the radial dependence, and k_m is the wavenumber describing the axial periodicity of the channel. Exact solutions to Eq. (2) exist for this profile, which simplifies analysis of electron beam dynamics. Once A_r has been determined, A_z and the axial electric field can be determined by $\vec{\nabla}\cdot\vec{A} \approx 0$, which is consistent with the assumption $\omega_p \ll \omega_0$. The slowly varying envelope approximation neglects second derivatives in z and t in the wave equation that are responsible for subluminal group velocity, but the group velocity can be explicitly restored by replacing $c^{-1}\partial/\partial t$ with $v_g^{-1}\partial/\partial t$ in Eq. (2). Here $v_g = 1 - \omega_{p,0}^2/2\omega^2 - 4/(k_0 w_{\text{ch}})^2$, and we define $\omega_{p,0}^2 = \langle\omega_p^2(0,z)\rangle_z$, where the angle brackets represent an average over z.The lowest eigenmode solution of Eq. (2) is

$$\hat{A}_r(r,z,t) = A_0\frac{r}{w_{\text{ch}}}e^{-r^2/w_{ch}^2 - (z - v_g t)^2/\sigma_z^2}\sum_n (i)^n J_n(\psi)e^{-i\psi + i(\delta k + n k_m)z}, \tag{3}$$

where $J_n(\psi)$ is the nth-order Bessel function, $\psi = \delta\omega_{p,0}^2/2c^2 k_0 k_m$, and $\delta k = -k_0^{-1}(\omega_{p,0}^2/2c^2 + 4/w_{\text{ch}}^2)$. The pulse has a Gaussian temporal shape with duration σ_z/v_g.

In Eq. (3), we view the laser pulse as a sum of simple spatial harmonics. Each spatial harmonic moves with its own constant phase velocity and amplitude. Matching the corrugation period to L_d is equivalent to matching the phase velocity of a spatial harmonic to the electron velocity. The harmonics have a relative amplitude given by $J_n(\psi)$ and the effective phase velocity $v_{p,n}$ for the nth spatial harmonic is $v_{p,n}/c = 1 - n k_m/k_0 + \omega_{p,0}^2/2\omega^2 + 4/(k_0 w_{ch})^2$, where an appropriate choice of n and k_m yields a slow-wave spatial harmonic ($v_p < c$) necessary for electron acceleration.

To determine a scaling law for direct electron acceleration, we consider an electron with initial conditions $(r,v_r) = (0,0)$ and $(z,v_z) = (z_0, v_{z,0})$, where $v_{z,0}$ is assumed to be close enough to c such that the electron remains in the accelerating phase of the quasi-matched field over the process of acceleration. For our experimental conditions of $(\omega_{p,0}/\omega_0)^2(k_0/k_m) \ll 1$ [16], $\psi \ll 1$, and $J_n(\psi) \sim \psi^n/2^n n!$. The amplitude of the spatial harmonics decreases quickly

with harmonic number, so we focus on the $n=1$ spatial harmonic and set $v_{p,1}=v_{z,0}$. Choosing z_0 to optimize acceleration and integrating the axial electric field over the pulse-length dephasing time $\sigma_z/(v_g-v_{z,0})$ using $v_{z,0}\approx c$, we obtain for the energy gain

$$\left.\frac{\Delta E}{m_e c^2}\right|_{\mathrm{DA}} \sim 4\delta a_0\left(\frac{\sigma_z}{w_{\mathrm{ch}}}\right)\left(\frac{\lambda_p}{\lambda}\right)^2\left(1+\frac{2\lambda_p^2}{\pi^2 w_{\mathrm{ch}}^2}\right)^{-2}, \quad (4)$$

where $\lambda_p=2\pi c/\omega_{p,0}$. The pulse-length dephasing time limits the interaction length. By comparison, the dephasing-limited energy gain for resonant laser-wakefield acceleration is [34]

$$\left.\frac{\Delta E}{m_e c^2}\right|_{\mathrm{WF}} \sim \frac{a_0^2}{(1+a_0^2/2)^{1/2}}\left(\frac{\lambda_p}{\lambda}\right)^2\left(1+\frac{\lambda_p^2}{\pi^2 w_{\mathrm{ch}}^2}\right)^{-1}. \quad (5)$$

For a wavelength of $\lambda=800$ nm, matched beam radius $w_{\mathrm{ch}}=15\ \mu$m, normalized amplitude $a_0=0.25$ corresponding to a laser power of 1.9 TW, pulse length $\sigma_z/c=300$ fs, on-axis plasma density $N_0=7\times10^{18}\ \mathrm{cm}^{-3}$, corrugation amplitude $\delta=0.9$, and modulation period of $T_m=349\ \mu$m (we use these parameters in our following calculations), we have $\Delta E/mc^2|_{\mathrm{DA}}\sim1000$. In [34], a 7.16 TW, 100 fs pulse in a suitable plasma channel yields $\Delta E/mc^2|_{\mathrm{WF}}\sim750$, a slightly reduced acceleration with similar pulse energy. However, it is with smaller lasers that direct acceleration (a linear process) has its strongest advantage: Replacing 1.9 TW with 30 GW would still give $\Delta E/mc^2|_{\mathrm{DA}}\sim125$, whereas (extremely nonlinear) wakefield acceleration is inoperable with such small lasers.

Equation (4) shows how important an optimized waveguide is for high-acceleration gradients. Acceleration is proportional to δ, so waveguides with sharp density structure, such as those shown in Fig. 5, may be ideal. Waveguide diameter is even more important; for fixed laser power, a smaller waveguide diameter w_{ch} will yield both a larger a_0 and a larger ratio of $E_{z,\mathrm{peak}}$ to $E_{r,\mathrm{peak}}$. Luckily, optically generated cluster-target waveguides can be precisely controlled, as shown in Figs. 3–5.

To study electron beam dynamics, we integrate the relativistic electron equations of motion in the laser electromagnetic field determined by Eqs. (1) and (3). We neglect space-charge effects, which become important when the axial electric field due to the bunched beam current becomes comparable to the quasi-phase-matched accelerating field. We estimate this gives an upper limit on the beam current of $I_{\max}[\mathrm{A}]<1.7\times10^4 a_0 J_1(\psi) w_{\mathrm{ch}}/\lambda$, which for our parameters is 3×10^4 A or 40 pC per microbunch.

Figures 8(a) and 8(b) show maximum particle energy gain versus time, for a pulse of duration $\sigma_z/c=300$ fs. The pulse-length dephasing time for this simulation is 130 ps. In Fig. 8(a), the effective phase velocity of the $n=1$ spatial harmonic is matched to three different initial electron velocities by tuning the modulation period, which could be accomplished experimentally by inserting imaging optics

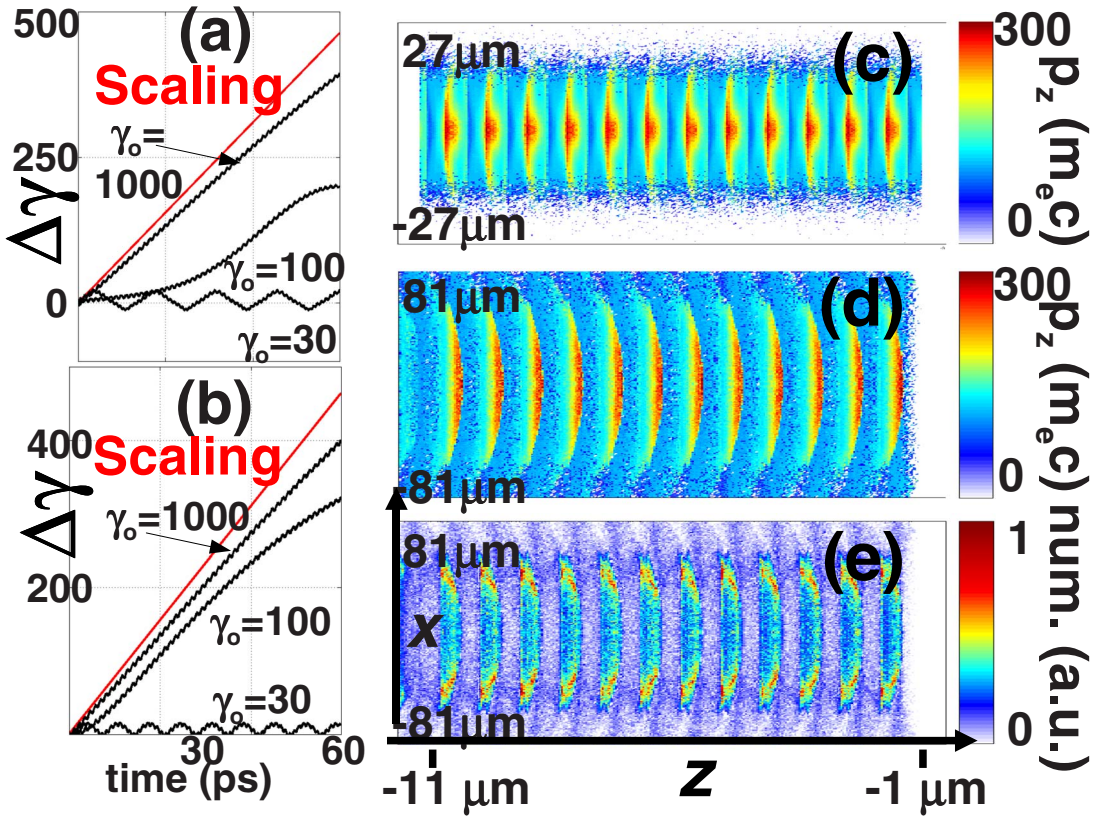

Fig. 8. (Color online) (a) Energy gain versus time with the slow-wave phase velocity matched to the initial electron velocity and (b) the slow-wave velocity is set to c. Allowing the electrons to catch up to the slow-wave velocity reduces the dephasing due to acceleration at higher energies. (c) Average final z momentum (color scale) as a function of initial position (z_0,x_0). (d) Average final z momentum (color scale) as a function of final position (z_f,x_f) relative to the leading electron. (e) Final electron density as a function of final position (z_f,x_f). The electron beam has become bunched and focused.

in the channel formation beam shown in Fig. 1. In Fig. 8(b), the phase velocity of the $n=1$ spatial harmonic was set to c for all three initial electron energies. The lines labeled scaling give the maximum energy gain based on the amplitude of the $n=1$ component of the axial electric field. Clearly it can be better to have electrons catch up to a slightly faster wave than for them to be initially resonant with, but eventually overtake, a slower one.

To examine transverse dynamics we distribute electrons uniformly in z from 1 to 11 μm behind the pulse maximum and with a Gaussian distribution in r with width σ_r. The pulse length is 300 fs. Figures 8(c) and 8(d) show the number-averaged final z momentum as a function of initial and final position, respectively, for an initial electron beam radius of 9 μm. Efficiency is very injector dependent: To be accelerated, electrons must start in buckets one half of a slow wavelength long and less than one laser spot size wide; for our parameters, the space-charge limit per bucket is <40 pC. Figure 8(e) shows the final electron beam density as a function of position; the beam has acquired a significant transverse spread that peaks off axis. Comparing Figs. 8(d) and 8(e), we see that these peaks are mostly composed of lower-energy electrons that have been expelled from the center of the buckets. These effects can be clearly seen in the linked multimedia file [35], which shows the time evolution of a subset of the particles from Figs. 8(c) and 8(d) in a window moving to the right at $\gamma=100$. The particle bunch is longer than one accelerating bucket; some electrons are decelerated and some are defocused. Electrons that do not accelerate slip into a defocusing region and are ejected from the waveguide. The highest-energy electrons simply plow ahead while absorbing energy, largely unaffected by transverse forces, and gain 151 MeV over 1.8 cm, a gradient of 84 MeV/cm. A 40 pC bucket would absorb approximately 6 mJ of energy, $\sim$1% of the driving pulse, while the number of loaded buckets depends on the injector. Since this acceleration process is linear and scales with the square root of laser power, a laser power of only 30 GW would yield a respectable gradient of 10.6 MeV/cm.

The fact that low-energy electrons are expelled from the waveguide suggests an interesting method to obtain high-quality monoenergetic electron beams from low-quality injected electrons. Study of Figs. 8(d) and 8(e) reveals that spatially filtering electrons at a radius greater than $\sim$20 μm would greatly decrease the number of low-energy electrons while leaving the high-energy electrons relatively unscathed. A carefully aligned pinhole following the waveguide thus might allow filtering of a low-quality injected beam. The injected beam will still heavily influence the quality of the accelerated electron beam, but the single-particle results shown in Fig. 8 allow simple estimation of how an injected beam will map to a final, accelerated beam for any given injector.

4. CONCLUSION

Two challenges remain: The generation of femtosecond, millijoule pulses of radially polarized light and the creation of a short, tightly focused electron bunch suitable for injection into our micrometer-scale structure. Efficient conversion of linearly polarized laser beams to radial polarization has been demonstrated for continuous-wave beams [36], and we are working to extend these results to femtosecond pulses. A simple, inexpensive electron injection technique is crucial to the success of electron acceleration with subterawatt lasers. Nonperiodic corrugations can phase match the acceleration of nonrelativistic electrons, but the minimum corrugation length gives a minimum electron injection speed. An injector based on either radio-frequency acceleration [37] or millijoule-level illumination of solid targets [38] could potentially produce an initial high-quality electron bunch fast enough to be injected without too much added expense.

In conclusion, we have demonstrated guiding and dispersive control of intense laser pulses in miniature plasma slow-wave guiding structures, making particle acceleration based on quasi phase matching possible. Our corrugated channel generation scheme, which exploits the unique properties of clusters and cluster plasmas, makes possible control of the dominant axial spatial harmonics of the driving waves. Our simulations show that this structure can allow truly tabletop lasers to accelerate electrons to high energies in short distances.

ACKNOWLEDGMENTS

This work was supported by the U.S. Department of Energy and the National Science Foundation. The authors thank C. Pesto for technical assistance.

REFERENCES

1. T. Tajima and J. M. Dawson, "Laser electron accelerator," Phys. Rev. Lett. **43**, 267–270 (1979).
2. E. Esarey, P. Sprangle, J. Krall, and A. Ting, "Overview of plasma-based accelerator concepts," IEEE Trans. Plasma Sci. **24**, 252–288 (1996).
3. V. Malka, S. Fritzler, E. Lefebvre, M.-M. Aleonard, F. Burgy, J.-P. Chambaret, J.-F. Chemin, K. Krushelnick, G. Malka, S. P. D. Mangles, Z. Najmudin, M. Pittman, J.-P. Rousseau, J.-N. Scheurer, B. Walton, and A. E. Dangor, "Electron acceleration by a wake field forced by an intense ultrashort laser pulse," Science **298**, 1596–1600 (2002).
4. "The light fantastic," The Economist, September 28, 2006.
5. S. P. D. Mangles, C. D. Murphy, Z. Najmudin, A. G. R. Thomas, J. L. Collier, A. E. Dangor, E. J. Divall, P. S. Foster, J. G. Gallacher, C. J. Hooker, D. A. Jaroszynski, A. J. Langley, W. B. Mori, P. A. Norreys, F. S. Tsung, R. Viskup, B. R. Walton, and K. Krushelnick, "Monoenergetic beams of relativistic electrons from intense laser–plasma interactions," Nature **431**, 535–538 (2004).
6. C. G. R. Geddes, Cs. Toth, J. van Tilborg, E. Esarey, C. B. Schroeder, D. Bruhwiler, C. Nieter, J. Cary, and W. P. Leemans, "High-quality electron beams from a laser wakefield accelerator using plasma-channel guiding," Nature **431**, 538–541 (2004).
7. J. Faure, Y. Glinec, A. Pukhov, S. Kiselev, S. Gordienko, E. Lefebvre, J.-P. Rousseau, F. Burgy, and V. Malka, "A laser–plasma accelerator producing monoenergetic electron beams," Nature **431**, 541–544 (2004).
8. W. P. Leemans, B. Nagler, A. J. Gonsalves, Cs. Tóth, K. Nakamura, C. G. R. Geddes, E. Esarey, C. B. Schroeder, and S. M. Hooker, "GeV electron beams from a centimetre-scale accelerator," Nat. Phys. **2**, 696–699 (2006).
9. B. D. Layer, A. York, T. M. Antonsen, S. Varma, Y.-H. Chen, Y. Leng, and H. M. Milchberg, "Ultrahigh-intensity optical slow-wave structure," Phys. Rev. Lett. **99**, 035001 (2007).

10. A. G. York, H. M. Milchberg, J. P. Palastro, and T. M. Antonsen, "Direct acceleration of electrons in a corrugated plasma waveguide," Phys. Rev. Lett. **100**, 195001 (2008).
11. http://www2.slac.stanford.edu/vvc/accelerators/structure.html.
12. A. Butler, A. J. Gonsalves, C. M. McKenna, D. J. Spence, S. M. Hooker, S. Sebban, T. Mocek, I. Bettaibi, and B. Cros, "Demonstration of a collisionally excited optical-field-ionization XUV laser driven in a plasma waveguide," Phys. Rev. Lett. **91**, 205001 (2003).
13. D. V. Korobkin, C. H. Nam, S. Suckewer, and A. Goltsov, "Demonstration of soft x-ray lasing to ground state in Li iii," Phys. Rev. Lett. **77**, 5206–5209 (1996).
14. H. M. Milchberg, C. G. Durfee III, and J. Lynch, "Application of a plasma waveguide to soft-x-ray lasers," J. Opt. Soc. Am. B **12**, 731–737 (1995).
15. H. M. Milchberg, C. G. Durfee III, and T. J. McIlrath, "High-order frequency conversion in the plasma waveguide," Phys. Rev. Lett. **75**, 2494–2497 (1995).
16. T. R. Clark and H. M. Milchberg, "Optical mode structure of the plasma waveguide," Phys. Rev. E **61**, 1954–1965 (2000).
17. L. Schachter, *Beam-Wave Interaction in Periodic and Quasi-Periodic Structures* (Springer, 1997).
18. R. H. Stolen and H. W. K. Tom, "Self-organized phase-matched harmonic generation in optical fibers," Opt. Lett. **12**, 585–587 (1987).
19. R. Kashyap, "Phase-matched periodic electric-field-induced second-harmonic generation in optical fibers," J. Opt. Soc. Am. B **6**, 313–328 (1989).
20. M. M. Fejer, G. A. Magel, D. H. Jundt, and R. L. Byer, "Quasi-phase-matched second harmonic generation: Tuning and tolerances," IEEE J. Quantum Electron. **28**, 2631–2654 (1992).
21. S. Chao, H.-Y. Chen, Y.-H. Yang, Z.-W. Wang, C. Shih, and H. Niu, "Quasi-phase-matched second-harmonic generation in Ge-ion implanted fused silica channel waveguide," Opt. Express **13**, 7091–7096 (2005).
22. A. Paul, R. A. Bartels, R. Tobey, H. Green, S. Weiman, I. P. Christov, M. M. Murnane, H. C. Kapteyn, and S. Backus, "Quasi-phase-matched generation of coherent extreme-ultraviolet light," Nature **421**, 51–54 (2003).
23. H. M. Milchberg, T. R. Clark, C. G. Durfee III, and T. M. Antonsen, "Development and applications of a plasma waveguide for intense laser pulses," Phys. Plasmas **3**, 2149–2155 (1996).
24. J. H. Cooley, T. M. Antonsen, H. M. Milchberg, J. Fan, L. Margolin, and L. Pyatnitskii, "Parametric instability in the formation of plasma waveguides," Phys. Rev. E **73**, 036404 (2006).
25. H. Sheng, K. Y. Kim, V. Kumarappan, B. D. Layer, and H. M. Milchberg, "Plasma waveguides efficiently generated by Bessel beams in elongated cluster gas jets," Phys. Rev. E **72**, 036411 (2005).
26. S. P. Nikitin, I. Alexeev, J. Fan, and H. M. Milchberg, "High efficiency coupling and guiding of intense femtosecond laser pulses in preformed plasma channels in an elongated gas jet," Phys. Rev. E **59**, R3839–R3842 (1999).
27. W. D. Kimura, G. H. Kim, R. D. Romea, L. C. Steinhauer, I. V. Pogorelsky, K. P. Kusche, R. C. Fernow, X. Wang, and Y. Liu, "Laser acceleration of relativistic electrons using the inverse Cherenkov effect," Phys. Rev. Lett. **74**, 546–549 (1995).
28. T. Plettner, R. L. Byer, E. Colby, B. Cowan, C. M. S. Sears, J. E. Spencer, and R. H. Siemann, "Visible-laser acceleration of relativistic electrons in a semi-infinite vacuum," Phys. Rev. Lett. **95**, 134801 (2005).
29. M. D. Perry and G. Mourou, "Terawatt to petawatt subpicosecond lasers," Science **264**, 917–924 (1994).
30. P. Serafim, P. Sprangle, and B. Hafizi, "Optical guiding of a radially polarized laser beam for inverse Cherenkov acceleration in a plasma channel," IEEE Trans. Plasma Sci. **28**, 1190–1193 (2000).
31. A. G. York, B. D. Layer, and H. M. Milchberg, "Application of the corrugated plasma waveguide to direct laser acceleration," AIP Conf. Proc. **877**, 807–811 (2006).
32. M. Xie, Lawrence Berkeley National Laboratory, Report 48236, "Plasma inverse transition acceleration" (2001).
33. A. Farjadpour, D. Roundy, A. Rodriguez, M. Ibanescu, P. Bermel, J. D. Joannopoulos, S. G. Johnson, and G. W. Burr, "Improving accuracy by subpixel smoothing in the finite-difference time domain," Opt. Lett. **31**, 2972–2974 (2006).
34. R. F. Hubbard, P. Sprangle, and B. Hafizi, "Scaling of accelerating gradients and dephasing effects in channel-guided laser wakefield accelerators," IEEE Trans. Plasma Sci. **28**, 1159–1164 (2000).
35. http://www.glue.umd.edu/~york/scatter-JOSAB.mpg
36. G. Machavariani, Y. Lumer, I. Moshe, A. Meir, and S. Jackel, "Efficient extracavity generation of radially and azimuthally polarized beams," Opt. Lett. **32**, 1468–1470 (2007).
37. T. van Oudheusden, E. F. de Jong, S. B. van der Geer, W. P. E. M. Op 't Root, O. J. Luiten, and B. J. Siwick, "Electron source concept for single-shot sub-100 fs electron diffraction in the 100 keV range," J. Appl. Phys. **102**, 093501 (2007).
38. T. Palchan, S. Eisenmann, A. Zigler, D. Kaganovich, R. F. Hubbard, M. Fraenkel, D. Fisher, and Z. Henis, "All optical electron injector using an intense ultrashort pulse laser and a solid wire target," Appl. Phys. B **83**, 219–223 (2006).